Waste Management 134 (2021) 231–240

Contents lists available at ScienceDirect

Waste Management

journal homepage: www.elsevier.com/locate/wasman

Characterization of MSWI fly ashes along the flue gas cooling path and implications on heavy metal recovery through acid leaching

M. Wolffers [a,*], U. Eggenberger [a], S. Schlumberger [b], S.V. Churakov [a,c]

[a] Institute of Geological Sciences, University of Bern, Switzerland
[b] Zentrum für nachhaltige Abfall- und Ressourcennutzung (ZAR), Zuchwil, Switzerland
[c] Laboratory for Waste Management, Paul Scherrer Institute, Villigen, Switzerland

ARTICLE INFO

Keywords:
Mineralogy of waste incineration residues
MSWI fly ash
Empty pass ash
Boiler ash
Electrostatic precipitator ash
Heavy metal recovery

ABSTRACT

This study reports on detailed chemical and mineralogical characterization of the different municipal solid waste incineration ashes forming along the flue gas path of plants with separate dust removal and neutralization. In pursuit of optimizing heavy metal recovery through acid leaching, the metal extractability from empty pass ashes (EA), boiler ashes (BOA) and the electrostatic precipitator ashes (ESPA) was evaluated and compared. The focus was laid on matrix phases affecting leachability (e.g. alkalinity, oxidation–reduction potential), as well as on distribution and concentration of recoverable heavy metals and their binding forms. The data showed, that EA and BOA are geochemically similar and are essentially composed of two different materials: the heavy metal poor airborne ash particles and the Zn- and Pb-rich sulfate deposits that condensate on heat exchanger surfaces. Variation in relative amount and chemical composition of the deposits is responsible for fluctuations in bulk composition of EA and BOA. The ESPA shows different chemical and mineralogical characteristics than EA and BOA. The ESPA is enriched in the volatile heavy metals Zn, Pb, Cu, Cd and Sn, which are mainly incorporated in chlorides and sulfates. The high content of salt-bound and thus easily soluble heavy metals together with the lower alkalinity and lower oxidation–reduction potential indicates, that ESPA has a better leachability compared to EA and BOA. The EA and BOA, on the other hand, do not show any significant differences in leachability. The data may contribute to a basis for re-evaluating disposal routes of ash fractions with poor extraction properties.

1. Introduction

Heavy metal recovery from residues of municipal solid waste incineration (MSWI) is a sustainable technology for returning valuable metals back into the raw materials cycle. In Switzerland, two main types of solid residues remain after MSW incineration at 800–1000 °C: the bottom ash (800,000 t/y) and the fly ash (FA, 80,000 t/y) (BAFU, 2019). During incineration, volatile compounds from waste materials are transformed into the gas phase that form the flue gas. The transfer of heavy metals to the gas phase is thereby favored by higher furnace temperatures, as well as elevated chlorine and sulfur concentration in the flue gas (Verhulst et al. 1996; Abanades et al., 2002; Morf et al. 2000; Belevi and Moench 2000; Jakob et al. 1996). The first solid residue from the flue gas path is the ash arising at the 2nd and 3rd pass, also called the empty pass ash (EA), which is often disposed together with the bottom ash (Fig. 1). After leaving the 3rd pass, the flue gas flows through the boiler, which is equipped with heat exchanger tubes. By passing the boiler, the flue gas is cooled from approximately 650 °C to 250 °C. The boiler and electrostatic precipitator act as dust removal systems, where the different boiler ashes (BOA) and the electrostatic precipitator ash (ESPA) arise. BOA and ESPA are usually collected together and referred to as FA. Gaseous compounds (mainly halogens e.g. HCl, as well as SO_2) are removed from the flue gas in a dry, semi-dry or wet flue gas cleaning system, before the clean gas (N_2, CO_2 and H_2O) is emitted through the chimney. Dry- and semi dry flue gas cleaning systems use additives as neutralizing chemicals and produce solid flue gas cleaning products. In other countries, these flue gas cleaning residues are often collected together with FA and the hazardous mixture is termed air pollution control residues (APCr) (Quina et al., 2008; Quina et al., 2018). The wet flue gas cleaning system consists of a multi-stage scrubber and the APCr arise in liquid form as scrub water. In a first stage, the flue gas is quenched with water, whereby mainly HCl, HF and NH_3 are dissolved to form the acid scrub water. In a further stage, sulfur oxides (SO_2, SO_3) and residual heavy metals are separated with the addition of NaOH,

* Corresponding author.
E-mail address: mirjam.wolffers@geo.unibe.ch (M. Wolffers).

https://doi.org/10.1016/j.wasman.2021.08.022
Received 22 December 2020; Received in revised form 1 August 2021; Accepted 13 August 2021

resulting in neutral or alkaline scrub water. The scrub waters can be used for heavy metal extraction (e.g. Zn, Cu, Pb, Cd) through acid FA leaching (e.g. FLUWA process (Bühler and Schlumberger, (2010)). When the plant is not equipped with a facility for acid leaching, the scrub waters can be discharged to surface water after precipitation of hydroxide sludge and neutralization, if quality requirements are met. Pure gypsum can be precipitated from the sulfate bearing alkaline scrub water in order to avoid landfilling of a potential secondary raw material.

At present, Swiss bottom ash and FA are deposited on landfills as they do not meet the quality requirements for recycling. The Swiss waste ordinance (Swiss Federal Council, 2015) prescribes the recovery of metals from the incineration residues before landfilling. The heavy metals from bottom ash are recovered using physical processes (e.g. magnetism, eddy current) until the non-ferrous metal content is below 1 wt%. For FA, chemical processes such as acid leaching (e.g. FLUWA process (Bühler and Schlumberger, 2010)) represent the state-of-the art for heavy metal recovery. The resulting ash slurry is filtered into a heavy metal enriched leachate that can be used for heavy metal recovery (Schlumberger et al., 2007) and a filter cake with reduced heavy metal content, which is deposited on landfills. The annual amount of filter cake deposited is often not gravimetrically recorded, but is calculated using the typical mass loss during acid leaching of approx. 25–30% (Bühler and Schlumberger, 2010; Weibel et al., 2021). The mobilization of the heavy metals is mainly dependent on the heavy metal binding form and the extraction conditions (e.g. pH, redox conditions (Eh), liquid to solid ratio, temperature). FA show a very high reduction potential during extraction due to the presence of metallic compounds (e.g. Al^0 in Al-foil). Oxidation of Al^0 by Cu^{2+} and Pb^{2+} during leaching at low pH value causes a reductive cementation of Pb and Cu (Weibel et al., 2017), making these metals unavailable for recovery. In order to suppress reductive cementation, an oxidizing agent is often added.

In pursuit of a circular economy, the heavy metal recovery efficiency from FA needs to be further improved. Further optimization in the heavy metal recovery rates can either be achieved by modified process conditions or by excluding ash fractions with poor extraction properties (e.g. high acid neutralizing capacity (ANC), high Al^0 content or heavy metals bound in poorly soluble form). The EA, the first ash arising at the flue gas cleaning system, is already deposited together with the bottom ash in most plants. A further step towards optimizing the heavy metal recovery process could be the exclusion of BOA fractions with poor extraction properties. As data basis for evaluating whether a separation of material flows could be expedient for better heavy metal recovery rates, it is important to understand the geochemical differences between the different ash fractions (EA, BOA and ESPA). The major part of studies on MSWI FA analyze ashes from electrostatic precipitators (e.g. Gilardoni et al., 2004; Eighmy et al., 1995; Le Forestier and Libourel, 1998; Mahieux et al., 2010; Sandell et al., 1996). In contrast, relatively few studies have addressed the chemical and mineralogical characterization of MSWI BOA (De Boom and Degrez, 2015; Allegrini et al., 2014; Hsiao et al., 2006; Bodénan et al., 2010) or the characterization of different ash fractions from one plant (Keppert et al. (2012)). Still, little is known about the characteristics of EA and about the differences in chemical and mineralogical composition of the ash fractions arising along the flue gas cooling path.

The present study focuses on a detailed chemical and mineralogical characterization of the different ash fractions arising along the flue gas cooling path. EA, BOA and ESPA were collected at 6 different MSWI plants in Switzerland. The investigated plants are equipped with boiler and electrostatic precipitator (ESP) as main dedusting system upstream of the flue gas scrubber (separate dust removal and neutralization). Using a broad combination of methods (XRF, XRD, SEM), the ashes were characterized with respect to the chemical and mineralogical composition of major- and minor phases. A special focus was laid on possible binding forms of the target heavy metals Zn and Pb. The ANC and the content of metallic aluminum (Al^0) were determined for each ash fraction as parameter to estimate the extraction behavior.

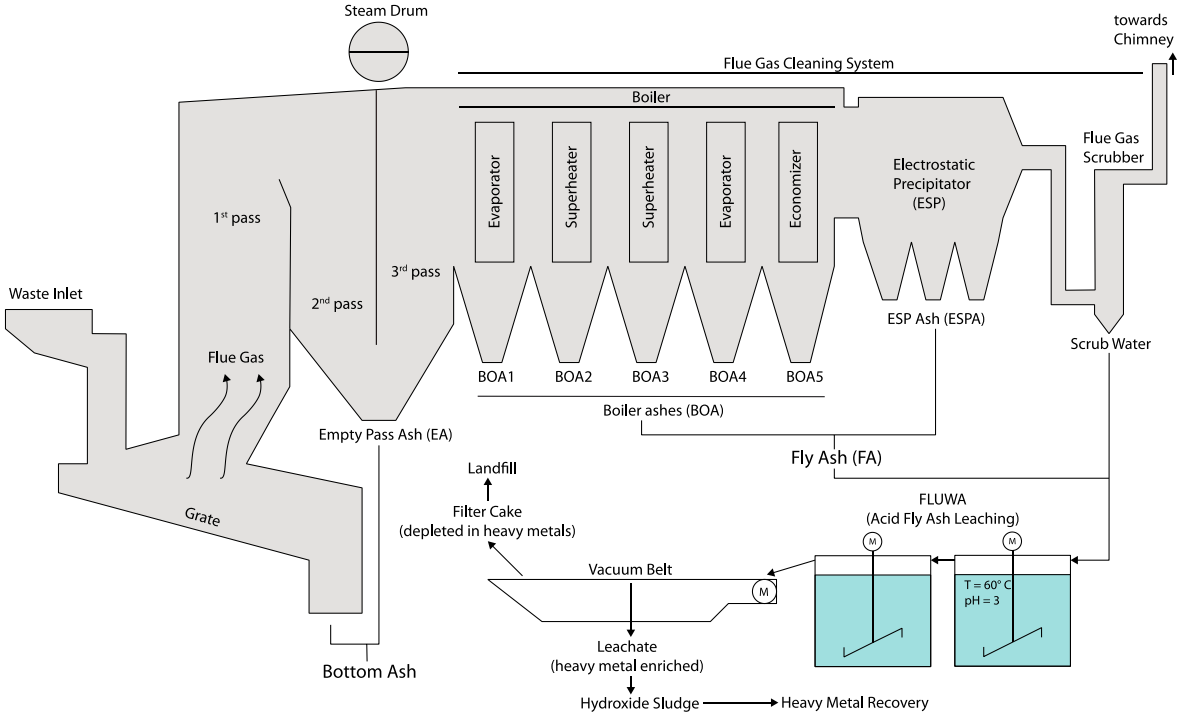

Fig. 1. Scheme showing the different mass streams arising from incineration, on the example of a wet flue gas cleaning system combined with acid fly ash leaching (FLUWA).
Adapted from Bühler and Schlumberger, 2010

2. Materials and methods

2.1. Characteristics of investigated plants

The majority of MSWI plants currently in operation in Switzerland are equipped with an electrostatic precipitator as pre-deduster and a wet flue gas cleaning system downstream of the boiler (AWEL, 2013). Accordingly, the six investigated Swiss MSWI plants (A-F) have similar flue gas cleaning systems with boiler and electrostatic precipitator (ESP) upstream of the flue gas scrubber, whereby dust removal and neutralization are performed separately. The plants A-E are equipped with a wet flue gas scrubber. Plant F is equipped with a dry flue gas scrubber and the neutralization residues are not collected with the FA but discharged separately. The plants show differences in boiler architecture (Fig. 2), waste throughput capacity and operating conditions (Table 1). All plants incinerate municipal-, as well as commercial- and industrial waste, partly also automobile shredder residues (ASR) and sewage sludge in small proportions (details in Table S1). The plant B incinerates mostly municipal waste (67%), while plant A incinerates increased amounts of industrial waste. For the other plants, the shares of municipal- and industrial waste are almost equal.

2.2. Sampling and sample preparation

The EA, BOA and ESPA were sampled in 6 different MSWI plants in Switzerland (A-F). Individual sampling strategies had to be developed and tuned for the different incinerator plants due to their differences in construction (Fig. 2). The EA could only be sampled at plant E and F (at the latter not in the same sampling period). In plant A and C there is no empty pass and BOA1 is discarded together with the bottom ash. The BOA fractions have been numbered such, that they originate from comparable boiler sections: BOA1 originates from the boiler hoppers below the evaporator and last superheater; BOA2 and BOA3 from hoppers below the superheaters; BOA4 from hoppers below the evaporator and BOA5 from hoppers below the economizer.

BOA was either retrieved after stowing ash material above manually closed pendulum flaps or collected by hanging a specially designed sampling holder in the outlet of each boiler hopper. For each increment, sampling was performed for a defined time (0.5–2 h) and several sampling increments of each boiler hopper were added to a heat-resistant container to form a composite sample per boiler hopper over several days to weeks (details in Table 1). ESPA was either discharged via the emergency ash removal system into a sample container or sampled off the conveyor belt and pooled into composite samples. Each composite sample was homogenized and split into 1 kg batches for further analysis. For selected plants, an aliquot of BOA1-3 was sieved with a 2 mm sieve in order to separate the airborne ash particles from the bulky deposits. The chemical and mineralogical analysis was then performed on both fractions in addition to the bulk material to understand the difference between the two materials.

2.3. Estimation of mass flows

A gravimetric determination of the amount of BOA produced per boiler hopper was not possible in any of the plants. Thus, the mass flows could only be estimated. Most of the sampled plants use a system of rapping gears that operate periodically (every few hours) in order to clean the heat exchanger surfaces from deposits. It was observed that the amount of BOA arising per boiler hopper decreased towards the end of the boiler when sampling without the operation of the rapping gears. However, when sampling with the operation of the rapping gears, different quantity distributions per hopper were observed, depending on the amount of material accumulated on the heat exchanger tubes. The percentage of BOA and ESPA with respect to the FA was calculated by means of the chemical composition. By knowing the chemical composition of the FA, the mass fraction of BOA and ESPA could be calculated for each element by solving for the smallest deviation from the FA concentration. The resulting mass fractions were then averaged. This resulted in a share of BOA in relation to the total amount of FA of 25–30 wt%. The quantity distribution within the boiler could not be determined because the chemical composition of the different BOA fractions was almost identical.

2.4. Chemical analysis

All ashes were dried at 105 °C to constant weight and ground to a particle size < 0.01 mm in a tungsten-carbide disk mill. Chemical composition of the matrix elements was determined by wavelength dispersive X-ray fluorescence analysis (WD-XRF) using a Panalytical Axios spectrometer on pressed powder pellets (40 mm diameter, 6.40 g material and 1.44 g wax as binder). The same pellets were analyzed with a Spectro Xepos spectrometer (ED-XRF) with matrix adjusted calibration for the heavy metals of interest (Zn, Cd, Cu, Pb). TOC was analyzed externally according to DIN 19539 on the dried and fine ground ash fractions used for chemical analysis. The content of Al^0 in the ashes was calculated from H_2 gas volume determination during oxidation of Al^0 with H_2O + NaOH, as described in Zucha et al., 2020.

2.5. Mineralogical analysis

For mineralogical analysis, a mixture of ash material (4 g) and corundum (1 g) as internal standard was ground in a XRD-Mill McCrone from Retsch for 6 min at 55 Hz to a grain size of 1–10 μm. The disoriented samples were then measured using a PANalytical X'Pert Pro diffractometer (CuKα-radiation) from 5 to 75° 2θ at 0.017°/step for 2h, with an acceleration voltage of 40 kV and an electron generating current of 40 mA. Rietveld refinements were performed with the TOPAS-Academic V6 software using the structural data (.cif files) of the Inorganic Crystal Structure Database (ICSD) as input.

2.6. Acid neutralizing capacity

Titration of the acid neutralizing capacity was performed on a mixture of ash (2 g) with 20 ml ultrapure water. The suspension was

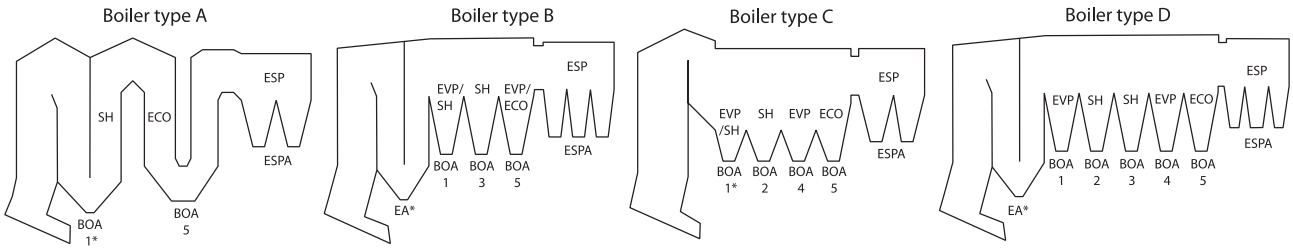

Fig. 2. Scheme of the different boiler types considered in this study with indications on the function of the different parts. EVP = evaporator, SH = superheater, ECO = economizer, ESP = electrostatic precipitator. Ash fractions marked with * are disposed together with the bottom ash.

Table 1
Operation details of the investigated MSWI plants and details on the different sampling campaigns.

Plant-ID	Boiler type	N° of increments/sampling duration	T combustion chamber (°C)	T boiler inlet (°C)	T boiler outlet (°C)	Incinerated waste (t/d)	Generated steam (t/h)
Plant A	A	28 incr./14d	925	650	195	330	55
Plant B	B	35 incr./50d	900	590	260	355	58
Plant C	C	2 incr./6 h	860	670	250	160	30
Plant D	D	21 incr./7d	840	635	274	400	75
Plant E	D	14 incr./14d	850	660	260	288	48
Plant F	D	9 incr./68 h	850	680	260	283	45

titrated in 40 steps using a 785 DPM Titrino device from Metrohm by adding 1 ml 1 M HCl in intervals of 10 min under constant stirring.

2.7. SEM microscopy

SEM analyses were performed on a Zeiss EVO-50 XVP electron microscope (SEM) coupled with an EDAX Apollo X energy dispersive system (EDS). The ash samples were embedded in epoxy resin, polished water-free and coated with carbon to avoid surface charging. An acceleration voltage of 15 kV, high vacuum mode and a spot size of 504 nm were used for backscattered electron (BSE) images.

3. Results

3.1. Chemical composition

The evolution in bulk chemical composition of the ashes arising along the flue gas cooling path shows trends that are similar for plants A-E (Fig. 3a). Elemental composition of EA and BOA are similar, but differ considerably from ESPA. BOA from plant F show a different trend in chemical composition and considerable differences in elemental concentrations and are therefore discussed separately.

In EA and BOA, Ca is the most abundant element (>200,000 mg/kg), followed by S (50–125,000 mg/kg). The EA and BOA further show Cl and Si as main constituents, followed by Na, K, Fe, Al (detailed in Table S2). The EA is thereby richer in Si, Al, Fe and lower in alkali, S, Cl than BOA. From BOA5 to ESPA, a major change in elemental composition can be observed, as there is a clearly visible drop in concentration of less volatile elements (Ca, Si, Al, Fe), complemented by a strong increase in more volatile elements (Cl, Na, K, Zn, Pb, Cu, Cd, Sb, Sn). The main constituents of ESPA are Cl, Ca, S, Na, K (>50,000 mg/kg). Volatile heavy metals of economic interest (e.g. Zn, Cu, Sn) and potentially environmentally hazardous heavy metals (e.g. Pb, Cd, Sb) are highly enriched in ESPA compared to EA and BOA. Nevertheless, Pb- and Sb peaks are also present in BOA3. The BOA from plant F show considerably lower Ca, Cl, Si, Al concentrations than the BOA from the other plants, but higher S, Na, K, Zn, Pb, Sb, Sn concentrations. A drop in Ca and an increase in Na, K concentration is observable from the middle of the boiler on and there is a strong Pb peak for BOA3, with concentrations almost 5x higher than in ESPA. Zn concentration in BOA from the rear part of the boiler are similar or higher than the Zn concentrations in ESPA from the other plants.

The concentration in total organic carbon (TOC) is generally higher for EA and BOA than for ESPA, but show big variation between the different plants and among the different ash fractions. There is no trend observable towards a decrease in flue gas direction within EA and BOA. Similarly, for the content of Al^0, there is no clear trend observable towards a decrease in flue gas direction within EA and BOA, except for plant F (Fig. 3b). Al^0 concentration in ESPA is significantly lower than in EA and BOA. Within EA and BOA from plant A-E, Al^0 concentrations vary between 2500 and 19,000 mg/kg, which represents 10–60% of the total Al content.

The deposits which were sieved from EA and BOA are characterized by high concentrations in S, Ca, Na and K, similar to the ashes from plant F (Fig. 4). Al, Fe, Si and Cl are present in minor concentrations. Only the deposits collected at the first boiler hopper from plants D and E show comparably high Cl concentrations. Zn, Pb, Cd concentrations are considerably higher in the deposits than in the corresponding BOA. Cu concentrations are equal or even lower in the deposits than in the bulk BOA.

3.2. Mineralogical composition and acid neutralizing capacity

The evolution in mineralogical composition of the airborne ash particles from EA, BOA and ESPA is very similar for plants A-E. Therefore, mineralogical composition along the flue gas cooling path is only shown for 2 plants with different boiler architecture (Fig. 5a, b) and for plant F, which shows different mineralogical composition (Fig. 5c).

EA and BOA show similar mineralogical composition (spectra in Fig. S1). The main components are anhydrite, silicates (e.g. the melilites gehlenite and akermanite, quartz and feldspars) and oxides (e.g. lime, hematite, perovskite). Calcite and chlorides (mainly halite) are also present in most EA and BOA, but in minor concentrations around 5 wt%. The portion of amorphous and unidentified phases was calculated to be 40–50%. The presence of amorphous or microcrystalline phases is clearly visible in the spectra by a background bump in the range between 20 and 40° 2Theta.

The EA from plant F shows a similar mineralogical composition than the EA from plant E. However, BOA from plant F show similar mineralogy as the deposits from plant E (Fig. 5c, d). The mineralogy is more sulfate-dominated and silicates represent minor constituents. There is a decrease in anhydrite concentration in flue gas direction, replaced by glauberite ($Na_2Ca(SO_4)_2$) as predominant sulfate from the middle of the boiler on. The complexity of the XRD spectra significantly increases from the 2nd to the 3rd boiler hopper, and associations of complex, possibly heavy metal bearing sulfate salts in minor concentrations are observed, displayed as “other sulfates”. A major phase in that category is the Zn- and Cl-bearing Na-sulfate d’ansite ($Na_{21}ZnCl_3(SO_4)_{10}$), which increases in concentration towards the end of the boiler and represents the only identified Cl-bearing phase. Other phases that increase towards the end of the boiler are K-bearing mixed sulfates (e.g. aphthitalite, alunite, K_2SO_4, K_2CaSO_4), which matches with the increase in K concentration from the 2nd to the 3rd pass. Pb sulfates (palmierite, anglesite), as well as Zn sulfates (K_2ZnSO_4, $ZnSO_4$) represent the heavy metal-bearing sulfates. Remarkably is the decrease in amorphous content in the ash from the last boiler hopper in BOA from plant F.

The ESPA are of different mineralogical composition than BOA and EA. The mineralogy is dominated by chlorides, matching the high Cl concentration. The spectra of the different ESPA is comparable (Fig. S1), but the absolute mineral concentrations vary from plant to plant. The mineralogy of the analyzed ESPA can be grouped into 3 types. ESPA from plant A, C and E show very high concentrations of halite (15–25 wt %) and K_2ZnCl_4 (9–16 wt%) and sylvite in minor concentrations. ESPA from plant D and F is characterized by high concentrations in K_2ZnCl_4 and d’ansite ($Na_{21}ZnCl_3(SO_4)_{10}$). Anhydrite and halite are present in concentrations around 10 wt%. ESPA from plant B does not contain K_2ZnCl_4. Instead, sylvite, calcite and oxide concentration are elevated in ESPA from plant B compared to other ESPA. For ESPA, the calculated amount for amorphous phases is as high as for BOA (approximately 50%). Although melt droplets can occasionally reach the electrostatic

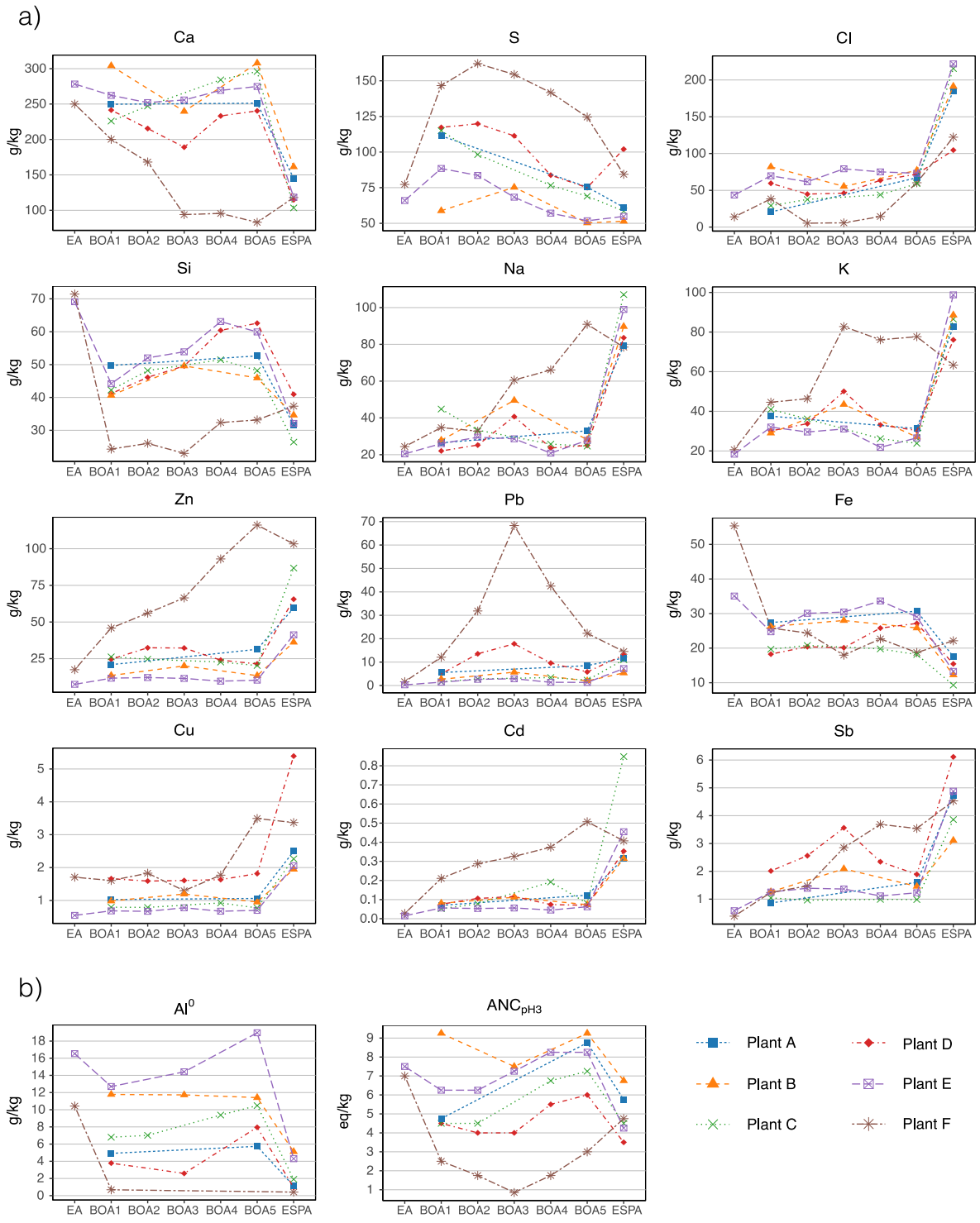

Fig. 3. (a) Evolution of bulk elemental composition along the flue gas cooling path, from the EA to the ESPA. (b) Evolution of the parameters affecting leachability: Al^0 concentration and ANC at pH 3, which represents the pH conditions of acid leaching.

precipitator, it has been observed by SEM investigations that ESPA is mainly composed of very fine crystals, probably too fine-grained (≪ 1 μm) to be resolved by XRD. It is therefore assumed, that unidentified microcrystalline phases make up for the major part of the amorphous or unidentified fraction.

As a result of the low concentration in acid-buffering minerals (e.g. CaO, $CaCO_3$, Ca-silicates), ESPA shows lower ANC than EA and BOA (Fig. 3b). ANC for EA and BOA are comparable and ANC of BOA from plant A-E show a slight increase towards the end of the boiler. For plant F, there is a significant drop in ANC from EA to BOA1. BOA from plant F show lower ANC than ESPA.

3.3. Morphology and particle chemistry

The morphological appearance of the airborne ash particles of EA and BOA is identical and only minor differences are identifiable between the different plants. The particle size distribution of EA and BOA varies from plant to plant, but remains relatively constant, with grain sizes

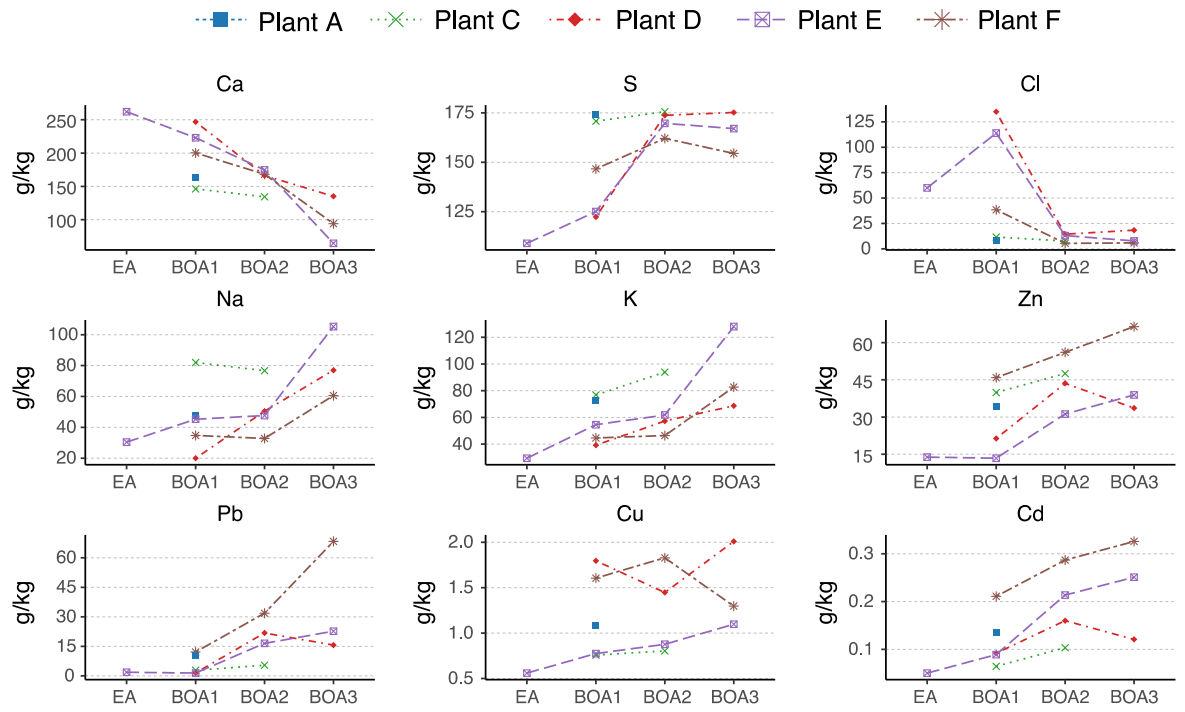

Fig. 4. Elemental composition of the deposits from plants A, C, D and E which were separated from the airborne ash particles by sieving. For comparison, the elemental composition of BA from plant F is shown.

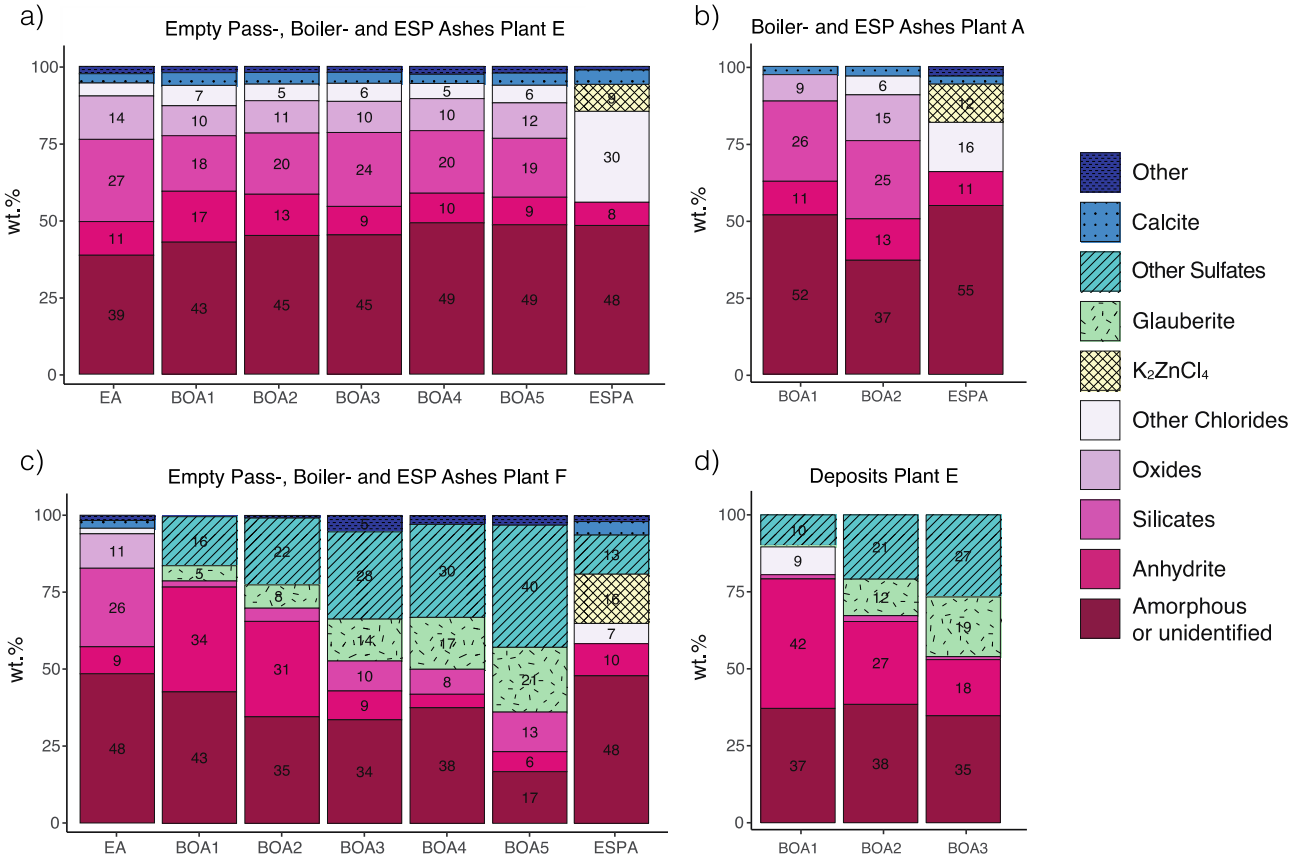

Fig. 5. Evolution of mineralogical composition along the flue gas cooling path for airborne ash particles (a, b, c) and deposits (d) from the different incineration plants. Only concentrations > 5 wt% are displayed as number.

ranging from 10 to 500 µm. It can be observed, that EA and BOA consist of three different phase types: refractory particles as well as newly formed particles in amorphous and crystalline form. The rounded shaped, porous amorphous phases represent a major part of the particles. These are mainly Fe- and Al- bearing Ca-silicates, which often contain to a lesser extent Mg, P, Ba or Ti. The chemical composition, as well as the shape and the porosity of the amorphous silicates vary broadly from particle to particle, and also compositional heterogeneities are observed within the particles. The characteristic dust rim covering the ash particles, which was previously observed in FA (Weibel et al., 2017), is not present in the BOA. However, the refractory particles often occur fully or partly covered with an amorphous or secondary formed fine crystalline phase. Among the observed refractory particles are rather inert minerals as quartz or feldspars and phases affecting the leaching behavior, as calcite and Al-foil (Fig. 6a, b). The calcite shows marginal decomposition features by loss of CO_2. Heavy metal enriched phases were mainly observed as segregation on amorphous silicate phases in BOA. They are often associated with Fe oxides close to the composition of hematite (Fe_2O_3) that segregate from amorphous particles, as also observed by other authors (Kutchko and Kim, 2006; Weibel et al., 2017). Ba, Ti, Ni, Cr and Zn were also found to be minor constituents of the Fe oxides. Fig. 6c shows such a coexistence of hematite and zinc ferrite (Fe_2ZnO_4) – a phase often observed in dusts from steel plants (Antrekowitsch et al., 2008). Zinc was also observed to be present as ZnO (Fig. 6d) and Zn_2SiO_4 around quartz particles (Fig. 6e). The observed newly formed phases are predominantly anhydrite and halite. They are found in large agglomerates, which can enclose amorphous melt droplets or refractory minerals. Often, complex mixed sulfates are found with large (Na,K)-$PbSO_4$ crystals, which were identified as fragments of deposits (Fig. 7b).

The BOA from plant F formed concentrically around the heat exchanger surfaces in direction of flue gas, with a dendritic appearance (Fig. 7a). Airborne ash particles accumulate between the “fingers”. The formation of the large (Na,K)-$PbSO_4$ crystals in parallel layers is well visible. Locally, the (Na,K)-$PbSO_4$ is formed antiparallel to the layering, which indicates migration and recrystallisation within the deposit. Crust fragments from plant D contain the same large (Na,K)-$PbSO_4$ crystals, as well as a Zn-bearing Na,K-sulfate matrix (Fig. 7b). The characteristic coexistence of sulfate matrices with different composition (e.g. $CaSO_4$ with (K)-$NaSO_4$) is shown in Fig. 7c. Also more complex matrix compositions close to the composition of $K_2Na_8Ca(SO_4)_6$, $K_2Na_2Zn(SO_4)_2$ or $Na_2K_2CaZn(SO_4)_4$ were observed.

ESPA shows different morphology than EA and BOA, characterized by very fine newly condensed crystals in the sub-micron scale (Fig. 7d), with the strong tendency of the individual ash particles to form agglomerates. Refractory minerals (e.g. quartz, calcite) can be observed, which are often partly covered with the fine-grained salt crystals. Small Al-foil fragments and melt droplets were observed in minor quantities. The EDX mapping (Fig. S2) of the particle agglomerate in Fig. 7e shows at this resolution a very homogeneous chemical composition over the entire particle agglomerate. The fine-grained ash particle matrix is composed of N, S, Ca, Zn, S, Cl and represents mixed chlorides and sulfates. $PbSO_4$ is distributed more punctually over the particle agglomerate, visible by the bright spots. The strong potential for particle agglomeration of ESPA and the very fine-grained nature of the ESPA complicates its characterization.

4. Discussion

4.1. Element partitioning and formation of the different ash fractions

The distribution of the chemical compounds along the cooling path is controlled by transport distance and formation mechanism. The fact that the Ca-, Si-, Fe-, Al-bearing glass- and refractory particles are mainly observed in EA and BOA suggests, that these particles are entrained with the flue gas and subsequently settle as they are transported through the empty pass and the boiler. However, refractory particles and melt

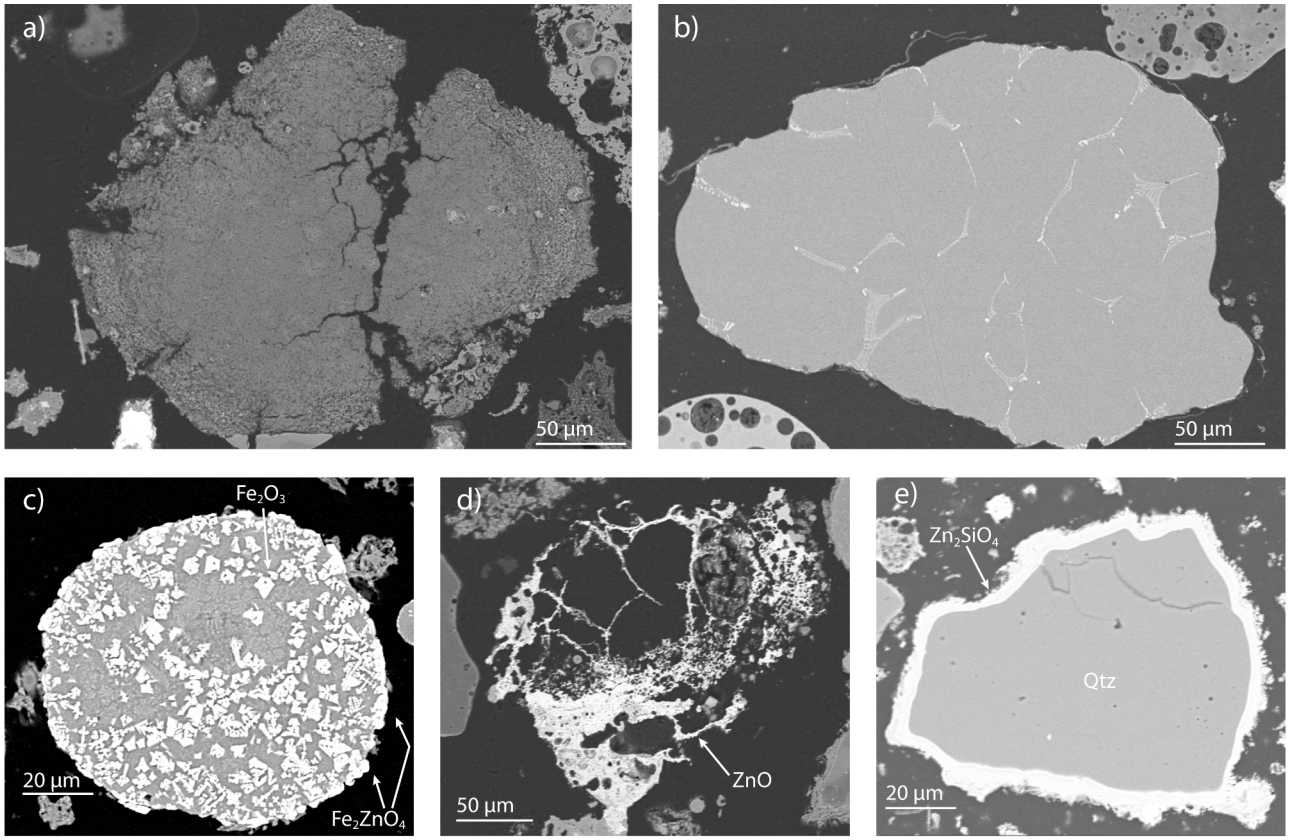

Fig. 6. Backscattered electron (BSE) images of refractory phases in BOA: calcite (a) and Al-foil (b), and different newly formed Zn phases observed in BOA (c)–(e).

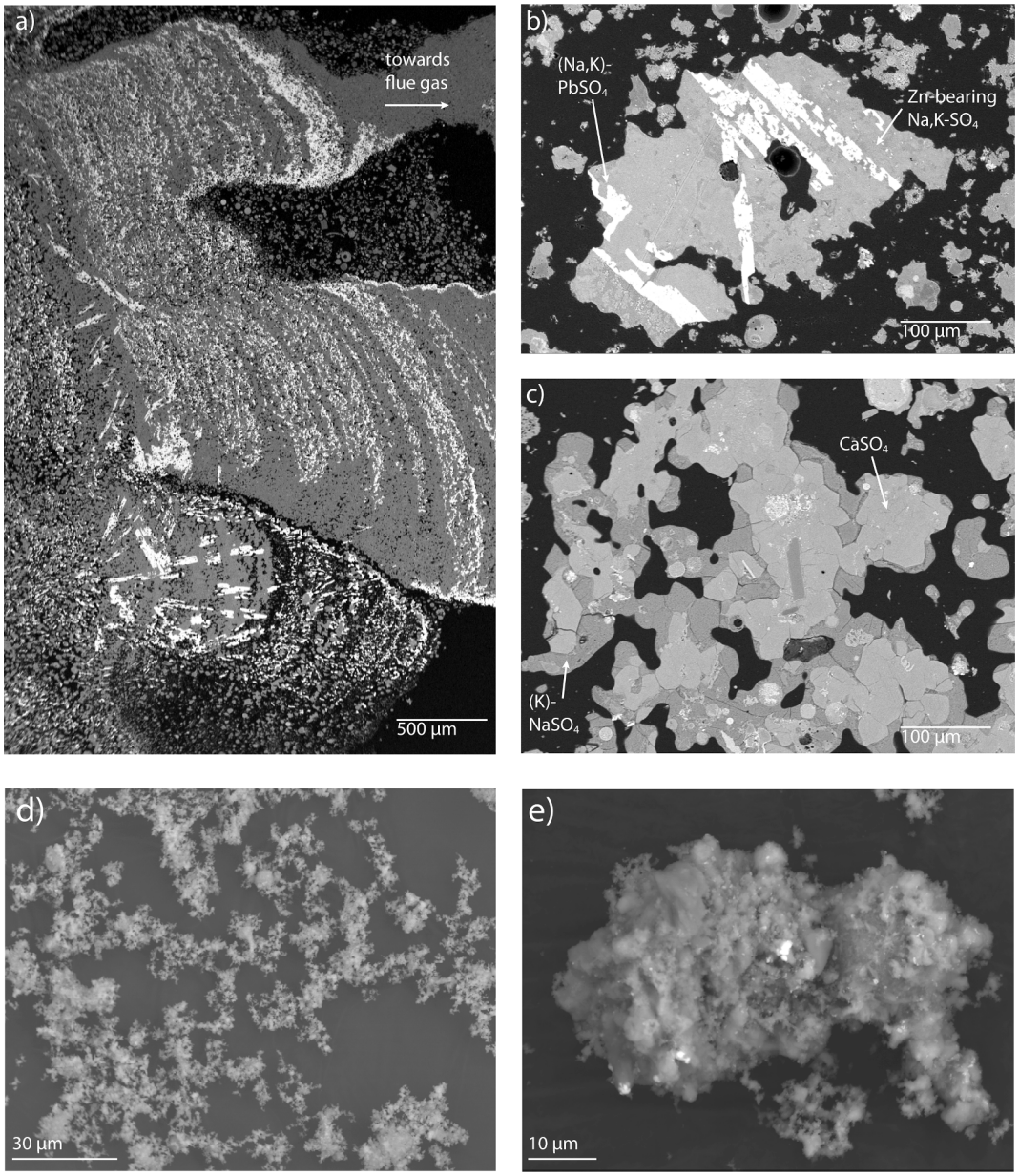

Fig. 7. Backscattered electron (BSE) images of deposits (a–c) and ESPA (d–e). Deposit-like BOA from plant F (a), particle piece of a deposit from plant D rich in $PbSO_4$ (b), coexistence of different matrix compositions (c). Individual particles (d) and particle agglomerate (e) of ESPA.

droplets occasionally reach the electrostatic precipitator, which explains the presence of Ca and Si in ESPA. Elements which form volatile compounds with high vapor pressures (e.g chlorides and sulfates) are observed to travel further until they precipitate at the ESP. The alkali metals Na, K and the heavy metals Zn, Pb, Cd are mainly observed in newly formed particles in the ESPA, which suggests that they are transported as gaseous compounds (e.g. as chlorides or sulfates). The distribution of the elements along the flue gas cooling path from this study fits well the observations made by Belevi and Moench (2000) and Morf et al., (2000) – even though they analyzed the BOA as a whole, not divided into the different fractions. It is further assumed, that the characteristic dust rims around glass- and refractory particles observed by Weibel et al., (2017) in FA represents ESPA. This would fit to the measured chemical composition of the dust rim, being rich in Cl, Zn, S, Na, K. The accumulation of ESPA around the bigger BOA grains could either result from impact milling or during storage, regarding the strong potential for particle agglomeration around bigger grains (Fig. 7e).

Fluctuations in the bulk elemental composition of EA and BOA are related to the amount of deposits contained in the ashes. The fact, that the deposits show higher heavy metal concentrations than the corresponding BOA shows that most heavy metals (especially Zn, Pb, Cd, Sb, Sn) tend to accumulate in the deposits rather than in the airborne BOA. Thus, the increased heavy metal contents in the BOA are mainly caused by the presence of the heavy metal enriched deposits. The macroscopic and microscopic appearance of the ashes from plant F (light brown, crumbly chunks), as well as the similar chemical and mineralogical composition, suggests that the BOA from plant F are mainly composed of heat exchanger deposits. As the EA from plant F is chemically and mineralogically similar the EA and BOA from the other plants, it is assumed, that a major part of the airborne ash particles of plant F already settle from the flue gas in the empty pass.

The condensation of volatile species on the walls and heat exchanger surfaces seems to be induced by locally favorable conditions. Due to the high Na, K, S concentration in the flue gas, it is mainly alkali sulfates that condensate on the walls and heat exchanger surfaces. It was observed that the formation of alkali sulfates occurred after oxidation from SO_2 to

sulfate which induced subsequent nucleation of alkali sulfates during cooling of the flue gas (Jensen et al., 2000). In some of the investigated incineration plants it was also observed that with increasing time from the last revision there was a shift of the S load in the boiler area from back to front, probably due to the deposits on the boiler walls and between the heat exchanger surfaces, which served as nucleation surface for supersaturated S compounds in the flue gas. It is therefore assumed that deposits are initially formed by local supersaturation due to the large temperature gradients between the hot flue gas and the tube surface. As soon as some layers of deposits exist, the temperature gradient decreases, but the nucleation area increases enormously, which favors the condensation of sulfate compounds. The coexistence of different sulfate matrices in the deposits might reflect differences in flue gas composition with time, resulting in a variation in composition of the condensates. Accordingly, high Zn vapor pressures may lead to the incorporation of Zn in the alkali sulfates. The conditions in the area of the superheater tubes seem to favor the condensation of $PbSO_4$, as the deposits grown on superheater tubes show the highest Pb concentration observed. The presence of $PbSO_4$ antiparallel to the layering (Fig. 7a) indicates, that recrystallisation processes occur within the deposits. In such deposits, sulfation reactions may occur which take place on the deposit surface, as well as inside the deposit (Grabke et al., 1995). Within these sulfation reactions, condensed chlorides are transformed to sulfates by substitution of the anion. The sulfation reactions are important for corrosion processes, since the transformation of chlorides to sulfates liberates the highly corrosive Cl and enables it to travel towards the boiler tube. There, it can attack the steel tubes and form $FeCl_2$ on the tube surface. The migration of the Cl toward the boiler tube through sulfation reactions could also explain the low Cl concentrations in the deposits because only the outer layer of the deposit is removed by the operation of the rapping gears.

4.2. Mineralogy and effects on extractability

The mineralogical composition of the EA, BOA and ESPA strongly influences the ANC. An interesting finding is the presence of calcite particles with decomposition features, as shown in Fig. 6a. This indicates that calcites were carried with the flue gas as refractory particles rather than that they formed secondarily from CaO. Decomposition of carbonates starts from 700 °C, but a fair number of calcite particles seem to persist the high temperatures. Although melilite concentrations of up to 15 wt% were identified with XRD in the BOA, neither gehlenite nor akermanite was observed by SEM. This suggest, that these minerals are present as very fine grained, newly formed crystals, that are readily available for dissolution. As a result of the high content in calcite and Ca-silicates in EA and BOA from plants A-E, ANC is significantly higher than in the BOA from plant F. The evolution of ANC along the flue gas cooling path stands in relation to the amount of deposits arising at the different boiler hoppers. The presence of deposits in EA and BOA results in a dilution of the strongly pH buffering ash matrix - yielding a lower ANC, since they consist mainly of sulfate salts with negligible pH buffering capacity. With decreasing amount of deposits arising in the BOA towards the end of the boiler, the ANC rises. The ashes from plant F showed a very low ANC, as they are predominantly composed of low acid-buffering sulfates. In contrast to the deposits, where Ca is mainly present as sulfates, ESPA also contains $CaCO_3$ and possibly amorphous Ca-silicates to a minor extent, which explains the higher ANC. Al represented the only identified metal in metallic form observed in EA, BOA and ESPA. Although it is likely that especially larger Al-foil particles are not transported far and settle shortly after leaving the combustion chamber, there was no trend observable that Al^0 concentration was higher in the EA or in the BOA from the first hoppers after the combustion chamber.

5. Conclusion

The obtained results provide important insights into the formation of the different ash fractions and its geochemical characteristics. Quenched melt droplets and refractory particles entrained by the flue gas mainly settle in the empty pass and along the boiler, whereas elements which form volatile compounds travel within the flue gas until the electrostatic precipitator, where a major part of the gaseous compounds condensate as ESPA. EA and BOA showed comparable bulk chemical and mineralogical composition. They were found to be composed of two significantly different materials: the airborne ash particles and deposits formed on the walls and heat exchanger surfaces. For the heavy metals of interest (Zn, Pb, Cu, Cd), only Zn bearing phases were found in the airborne particles of the BOA (as ZnO, $ZnSiO_3$ as rim around refractory particles, and also as segregations from amorphous phases (e.g. Fe_2ZnO_4)). It is mainly the deposits that contribute to the elevated heavy metal concentration, explained by the well-developed, large (Na,K)-$PbSO_4$ crystals and the Zn-bearing matrix sulfates. The variation in the amount and chemical composition of the deposits controls the fluctuations in the bulk composition of EA and BOA. ESPA differed considerably in chemical and mineralogical composition from EA and BOA. The ESPA is enriched in the heavy metals Zn, Pb, Cu, Cd and Sn, which are mainly incorporated in newly formed chlorides and sulfates.

Among ESPA, EA and BOA, the ESPA has the highest heavy metal concentrations. It is therefore ESPA that contribute to the elevated heavy metal concentrations in FA – and the fact, that FA is composed of 70–75% ESPA. The high ANC and Al^0 content in EA and BOA will result in a higher consumption of neutralizing chemicals during acid leaching compared to ESPA. In addition, ESPA shows much higher concentrations in the heavy metals of interest (Zn, Cd, Cu, Pb), predominantly in the form of easily soluble salts. These observations suggest that individual treatment of ESPA has higher potential for heavy metal recovery. Comparing the EA and BOA, however, no significant differences could be found in the parameters affecting extractability. Therefore, no conclusive recommendation can be made as to which BOA fractions could be excluded from the acid leaching process. The mass flows could be considered as indicative criteria for excluding ash fractions, as comparatively little material is produced from the rear hoppers of the boiler.

Further optimization of the metal recovery could be achieved with a better understanding of thermodynamic and chemical equilibria along the gas cooling path. Geochemical modelling may help to reveal thermodynamic and kinetic factors controlling the formation of deposits and the geochemical interactions occurring during flue gas cooling. The application of higher-resolution instruments is suggested for a more detailed characterization of ESPA and for the investigation of possible binding partners of Cu and Cd.

Declaration of Competing Interest

The authors declare that they have no known competing financial interests or personal relationships that could have appeared to influence the work reported in this paper.

Acknowledgements

The work presented in this paper was financed by the Federal Office for the Environment (FOEN) and contributions from incineration plants. We thank the MSWI plant operators for providing sample material and information about their operating conditions. Many thanks to Gisela Weibel (University of Bern) for proof reading the manuscript. Analytical support by Alfons Berger, Anna Zappatini, Wolfgang Zucha and Christine Lemp (University of Bern), Christoph Neururer (University of Fribourg) and Stephan Fromm (ZAR) is highly acknowledged.

Appendix A. Supplementary material

Supplementary data to this article can be found online at https://doi.org/10.1016/j.wasman.2021.08.022.

References

Abanades, S., Flamant, G., Gagnepain, B., Gauthier, D., 2002. Fate of heavy metals during municipal solid waste incineration. Waste Manag. Res. 20 (1), 55–68. https://doi.org/10.1177/0734242X0202000107.

Allegrini, E., Boldrin, A., Jansson, S., Lundtorp, K., Fruergaard Astrup, T., 2014. Quality and generation rate of solid residues in the boiler of a waste-to-energy plant. J. Hazard. Mater. 270, 127–136. https://doi.org/10.1016/j.jhazmat.2014.01.048.

Antrekowitsch, J., Griessacher, T., Offenthaler, D., Schnideritsch, H., 2008. Charakterisierung und Verhalten von Zink-, Blei- und Halogenverbindungen beim Recycling von ElektrolichtbogenofenstäubenCharacterization and Behaviour of Zinc-, Lead- and Halogen Compounds during the Recycling of Electric Arc Furnace Dusts. Berg- und Hüttenmännische Monatshefte 153 (5), 182–188. https://doi.org/10.1007/s00501-008-0372-7.

Amt für Abfall, Wasser, Energie und Luft (AWEL), 2013. Stand der Technik für die Aufbereitung von Rauchgasreinigungsrückständen (RGRR) aus Kehrichtverbrennungsanlagen.

Belevi, H., Moench, H., 2000. Factors determining the element behavior in municipal solid waste incinerators. 1. Field studies. Environ. Sci. Technol. 34 (12), 2501–2506. https://doi.org/10.1021/es991078m.

Bodénan, F., Guyonnet, D., Piantone, P., Blanc, P., 2010. Mineralogy and pore water chemistry of a boiler ash from a MSW fluidized-bed incinerator. Waste Manag. 30 (7), 1280–1289. https://doi.org/10.1016/j.wasman.2010.01.020.

Bundesamt für Umwelt (BAFU), 2019. Vollzugshilfe für die «Rückgewinnung von Metallen aus den Filteraschen von Kehrichtverwertungsanlagen». Bundesamt für Umwelt, Bern. Umwelt-Vollzug Nr.1826: 21 S.

Bühler, A., Schlumberger, S., 2010. Schwermetalle aus der Flugasche zurückgewinnen « Saure Flugaschewäsche – FLUWA-Verfahren » ein zukunftsweisendes Verfahren in der Abfallverbrennung. KVA-Rückstände der Schweiz. Der Rohstoff mit Mehrwert (Bundesamt für Umwelt BAFU), pp. 185–192.

De Boom, A., Degrez, M., 2015. Combining sieving and washing, a way to treat MSWI boiler fly ash. Waste Manag. 39, 179–188. https://doi.org/10.1016/j.wasman.2015.01.040.

Eighmy, T.T., Eusden, J.D., Krzanowski, J.E., Domingo, D.S., Staempfli, D., Martin, J.R., Erickson, P.M., 1995. Comprehensive approach toward understanding element speciation and leaching behavior in municipal solid waste incineration electrostatic precipitator ash. Environ. Sci. Technol. 29 (3), 629–646. https://doi.org/10.1021/es00003a010.

Gilardoni, S., Fermo, P., Cariati, F., Gianelle, V., Pitea, D., Collina, E., Lasagni, M., 2004. MSWI fly ash particle analysis by scanning electron microscopy-energy dispersive X-ray spectroscopy. Environ. Sci. Technol. 38 (24), 6669–6675. https://doi.org/10.1021/es0494961.

Grabke, H.J., Reese, E., Spiegel, M., 1995. The effects of chlorides, hydrogen chloride, and sulfur dioxide in the oxidation of steels below deposits. Corros. Sci. 37 (7), 1023–1043. https://doi.org/10.1016/0010-938X(95)00011-8.

Hsiao, M.C., Wang, H.P., Chang, J.-E., Peng, C.Y., 2006. Tracking of copper species in incineration fly ashes. J. Hazard. Mater. 138 (3), 539–542. https://doi.org/10.1016/j.jhazmat.2006.05.087.

Jakob, A., Stucki, S., Struis, R.P.W.J., 1996. Complete heavy metal removal from fly ash by heat treatment: influence of chlorides on evaporation rates. Environ. Sci. Technol. 30, 3275–3283. https://doi.org/10.1021/es960059z.

Jensen, J.R., Nielsen, L.B., Schultz-Møller, C., Wedel, S., Livbjerg, H., 2000. The nucleation of aerosols in flue gases with a high content of alkali – a laboratory study. Aerosol Sci. Technol. 33 (6), 490–509. https://doi.org/10.1080/02786820050195340.

Keppert, M., Pavlík, Z., Tydlitát, V., Volfová, P., Švarcová, S., Šyc, M., Cerný, R., 2012. Properties of municipal solid waste incineration ashes with respect to their separation temperature. Waste Manag. Res. 30, 1041–1048. https://doi.org/10.1177/0734242X12448513.

Kutchko, B., Kim, A., 2006. Fly ash characterization by SEM-EDS. Fuel 85 (17-18), 2537–2544. https://doi.org/10.1016/j.fuel.2006.05.016.

Le Forestier, Lydie, Libourel, Guy, 1998. Characterization of flue gas residues from municipal solid waste combustors. Environ. Sci. Technol. 32 (15), 2250–2256. https://doi.org/10.1021/es980100t.

Mahieux, P.-Y., Aubert, J.-E., Cyr, M., Coutand, M., Husson, B., 2010. Quantitative mineralogical composition of complex mineral wastes – contribution of the Rietveld method. Waste Manag. 30 (3), 378–388. https://doi.org/10.1016/j.wasman.2009.10.023.

Morf, Leo S., Brunner, Paul H., Spaun, Sebastian, 2000. Effect of operating conditions and input variations on the partitioning of metals in a municipal solid waste incinerator. Waste Manag. Res. 18 (1), 4–15. https://doi.org/10.1034/j.1399-3070.2000.00085.x.

Quina, Margarida J., Santos, Regina C., Bordado, João C., Quinta-Ferreira, Rosa M., 2008. Characterization of air pollution control residues produced in a municipal solid waste incinerator in Portugal. J. Hazard. Mater. 152 (2), 853–869. https://doi.org/10.1016/j.jhazmat.2007.07.055.

Quina, M.J., Bontempi, E., Bogush, A., Schlumberger, S., Weibel, G., Braga, R., Funari, V., Hyks, J., Rasmussen, E., Lederer, J., 2018. Technologies for the management of MSW incineration ashes from gas cleaning: new perspectives on recovery of secondary raw materials and circular economy. Sci. Tot. Env. 635, 526–542. https://doi.org/10.1016/j.scitotenv.2018.04.150.

Sandell, J.F., Dewey, G.R., Sutter, L.L., Willemin, J.A., 1996. Evaluation of lead-bearing phases in municipal waste combustor fly ash. J. Environ. Eng.

Schlumberger, S., Schuster, M., Ringmann, S., Koralewska, R., 2007. Recovery of high purity zinc from filter ash produced during the thermal treatment of waste and interting of residual materials. Waste Manag. Res. 25, 547–555.

Swiss Federal Council, 2015. Ordinance on the Avoidance and the Disposal of Waste. (Waste Ordinance, ADWO). (Status of 1 April 2020).

Verhulst, D., Buekens, A., Spencer, P.J., Eriksson, G., 1996. Thermodynamic behavior of metal chlorides and sulfates under the conditions of incineration furnaces. Environ. Sci. Technol. 30, 50–56. https://doi.org/10.1021/es940780+.

Weibel, Gisela, Eggenberger, Urs, Schlumberger, Stefan, Mäder, Urs K., 2017. Chemical associations and mobilization of heavy metals in fly ash from municipal solid waste incineration. Waste Manag. 62, 147–159.

Weibel, G., Zappatini, A., Wolffers, M., Ringmann, S., 2021. Optimization of metal recovery from MSWI fly ash by acid leaching: findings from laboratory- and industrial-scale experiments. Processes 9, 352. https://doi.org/10.3390/pr9020352.

Zucha, W., Weibel, G., Wolffers, M., Eggenberger, U., 2020. Inventory of municipal solid waste incineration fly ash in Switzerland: heavy metal recovery potential and their properties for acid leaching. Processes 8, 1668. https://doi.org/10.3390/pr8121668.